Time expansion in distributed optical fiber sensing

María R. Fernández-Ruiz, Miguel Soriano-Amat, Vicente Durán, Hugo F. Martins, Sonia Martin-Lopez, and Miguel Gonzalez-Herraez

(Invited paper)

***Abstract*—Distributed optical fiber sensing (DOFS) technology has recently experienced an impressive growth in various fields including security, structural monitoring and seismology, among others. This expansion has been accompanied by a speedy development of the technology in the last couple of decades, reaching remarkable performance in terms of sensitivity, range, number of independent sensing points and affordable cost per monitored point as compared with competing technologies such as electrical or point optical sensors. Phase-sensitive Optical Time-Domain Reflectometry (φOTDR) is a particularly interesting DOFS technique, since it enables real-time monitoring of dynamic variations of physical parameters over a large number of sensing points. Compared to their frequency-domain counterparts (OFDR), φOTDR sensors typically provide higher dynamics and longer ranges but significantly worse spatial resolutions. Very recently, a novel φOTDR approach has been introduced, which covers an existing gap between the long range and fast response of φOTDR and the high spatial resolution of OFDR. This technique, termed time-expanded (TE) φOTDR, exploits an interferometric scheme that employs two mutually coherent optical frequency combs. In TE-φOTDR, a probe comb is launched into the fiber under test. The beating of the backscattered light and a suitable LO comb produces a multi-heterodyne detection process that compresses the spectrum of the probe comb, in turn expanding the detected optical traces in the time-domain. This approach has allowed sensing using φOTDR technology with very high resolution (in the cm scale), while requiring outstandingly low detection and acquisition bandwidths (sub-MHz). In this work, we review the fundamentals of TE-φOTDR technology and describe the recent developments, focusing on the attainable sensing performance, the existing trade-offs and open working lines of this novel sensing approach.**

***Index Terms*—Dual frequency comb, modulation coding, optical time-domain reflectometry, scattering Rayleigh, quasi-integer-ratio.**

I. Introduction

DISTRIBUTED optical fiber sensing (DOFS) is a powerful technique that turns an optical fiber into a long sequence of "virtual sensors" able to localize and measure perturbations on physical parameters such as strain, temperature or vibrations [1–3]. DOFS delivering real-time measurements of dynamic perturbations, also known as distributed acoustic sensing (DAS) has recently gained much attention from both scientific and industrial communities due to its capacity to measure over long sensing ranges with fast update rate. State-of-the-art DAS systems offer sensing distances of tens of kilometers with resolutions of a few meters and acoustic sampling rates in the kilohertz range. The optical fibers involved in these systems, therefore, can be viewed as arrays of more than 10^3 sensors that are distributed every several meters and provide about 10^3 measurements per second. Even more, by combining DAS with distributed amplification, sensing ranges beyond 100 km are attainable, while preserving spatial resolutions below 10 m [4]. All these features have been exploited in a growing number of areas, such as surveillance, structural health monitoring, oil and gas industries and seismology [5–8].

A conventional DAS system relies on the detection of Rayleigh backscattering when optical pulses travel through an optical fiber. The weak return signal originated by the light propagation is due to the existence of small, randomly distributed refractive index fluctuations along the fiber [1]. The

Manuscript received xxxxx, revised xxy xxx; accepted xx xx. Date of publication xx; date of current version xx. The work of MRFR and HFM was supported by the MCIN/AEI/10.13039/501100011033 and European Union NextGenerationEU»/PRTR under grants RYC2021-032167-I and RYC2021-035009-I. The work of MSA and VD was supported by MCIN/AEI/10.13039/501100011033 and the FSE invierte en tu futuro under grants PRE-2019-087444 and RYC-2017-23668, respectively. This work was supported in part by Comunidad de Madrid and Feder Program under grant SINFOTON2-CM: S2018/NMT-4326, in part by Generalitat Valenciana under Grant PROMETEO/2020/029, in part by the Universitat Jaume I under Grant UJI-B2022-53, in part by the Spanish MCIN/AEI/10.13039/501100011033 and the European Union NextGenerationEU/PRTR Program under Grants PSI ref. PLEC2021-007875, and TREMORS ref. CPP2021-008869, in part by the Spanish MCIN/AEI/10.13039/501100011033 and FEDER Una manera de hacer Europa under grants PID2021-128000OB-C21, PID2021-128000OB-C22 and PID2021-124814NB-C22, in part by the European Innovation Council under Grant SAFE: ref. 101098992, *(Corresponding author: María R. Fernández-Ruiz)*

María R. Fernández-Ruiz, Miguel Soriano-Amat, Sonia Martin-Lopez, and Miguel Gonzalez-Herraez are with the Universidad de Alcalá, 28805 Alcalá de Henares, Spain, (e-mail: rosario.fernandezr@uah.es; miguel.soriano@uah.es; sonia.martinlo@uah.es; miguel.gonzalezh@uah.es).

Hugo F. Martins is with the Instituto de Óptica "Daza de Valdés", IO-CSIC, 28006 Madrid, Spain (e-mail: hugo.martins@csic.es).

Vicente Durán is with the GROC-UJI, Institute of New Imaging Technologies, University Jaume I, 12071 Castellón, Spain (e-mail: vduran@uji.es).

distribution of these inhomogeneities (or scattering centers) is sensitive to external perturbations such as temperature or strain, so the detection and analysis of the backscattered signal using reflectometry schemes can be exploited as distributed sensing mechanism. Among the different techniques based on Rayleigh scattering, phase-sensitive optical time-domain reflectometry (φOTDR) has aroused great interest due to its ability to spatially detect and measure dynamic variations of temperature and strain [1,2,5]. φOTDR requires a narrow-linewidth light source, resulting in a distributed fiber sensor that allows monitoring the phase of the backscattered light using different probe signals (individual, dual or chirped pulses) by direct or coherent detection [9–12].

φOTDR shows a fundamental trade-off between the signal-to-noise ratio (SNR) of the measured signals and the achievable spatial resolution. Due to the weakness of Rayleigh backscattering, high power pulses must be launched into the fiber, especially when considering long sensing distances. The input light peak power, however, is limited by the onset of nonlinearities [13]. If short pulses interrogate the fiber to attain a high spatial resolution, the existence of a power limitation leads to a low pulse energy, degrading the SNR [3]. To overcome this drawback, techniques based on trains of coded pulses have been proposed to increase the energy efficiency [14–16], demonstrating centimeter resolutions over kilometer ranges. In all cases, sub-nanosecond optical pulses demand fast photodetectors, expensive digitization electronics and high-capacity acquisition cards to cope with enormous amounts of data. For instance, a DAS sensor with a spatial resolution of 2 cm needs a detection bandwidth of at least 5 GHz and, therefore, an acquisition card with a sampling rate higher than 10 GSa/s, leading to a data rate beyond 80 GBps (assuming double-precision floating-point valued samples).

DAS implementations based on optical frequency-domain reflectometry (OFDR) have also been proposed [2,17]. Typically, OFDR has enabled DOFS measurements with very high resolution (even sub-mm) although with low update rate (of hertzs or below) and short sensing ranges, due to the need for frequency-scanning of the laser source over broad spectral ranges [2]. To attain dynamic performance over relatively long fiber ranges, an OFDR architecture based on a fast-scanning laser and coherent detection has been proposed in [17], providing kHz acoustic sampling in measurements along 10 km of fiber. However, the resolution was degraded to 10 m, reaching performance similar to that of φOTDR configurations. Another way of increasing the sampling rate in OFDR is through intra-scan algorithms [18], which deliver kHz acoustic bandwidth with tens of cm resolution, although severely limiting the attainable range (e.g., to a few meters).

Recently, we have proposed a novel distributed sensing technique, called time-expanded phase sensitive OTDR (TE-φOTDR), based on a coherent scheme that employs optical frequency combs (OFCs). From the beginning of the century, OFCs (optical spectra composed of a set of evenly spaced coherent lines) have caused a major impact in the field of photonics, since they can provide a direct link between optical and microwave frequencies [19]. In some areas, the ability of frequency combs to retrieve the spectral response of a sample is fully exploited by means of systems that involve two mutually coherent OFCs [20]. This dual-comb scheme has been implemented with a variety of OFC platforms for applications such as molecular spectroscopy and distance ranging [21–24]. In the case of distributed fiber sensing, high spatial resolutions over long distances require the creation of spectra composed of thousands of lines separated by very small spacing (from 10 MHz down to about 10s of kHz). This kind of ultra-dense OFCs can be generated by the electro-optic (EO) modulation of a continuous wave laser [25]. In EO dual-comb systems, the probe and the LO are generated from the same laser, ensuring an excellent high passive mutual coherence by construction. The result is a robust and flexible scheme that can be implemented with standard telecommunication equipment [26–28].

In TE-φOTDR, a custom-designed frequency comb is generated to probe a sensing fiber. The Rayleigh backscattered signal originated by the propagation of the probe is then mixed with a second comb, acting as local oscillator (LO), which has a slightly different line spacing [29,30]. This probe-LO configuration is known as dual frequency comb (DFC). After a multi-heterodyne detection process, the dual comb interference leads to a down-conversion of the optical frequencies into the radiofrequency domain, thus reducing the bandwidth of the detected signals in several orders of magnitude. In [29], for instance, a spatial resolution of 2 cm can be attained from a RF signal digitized at less than 10 MBps, which implies a reduction of at least 10^3 in the acquisition rate when compared to a traditional high-resolution φOTDR.

To date, the use of a DFC in DOFS has been tested just in a scheme based on phase-demodulation φOTDR. However, this approach could be readily implemented in other DOFS configurations, e.g., in wavelength-sweeping φOTDR schemes [31, 32]. Hence, by using the periodic probe signal and beating the backscattering signal with a suitable LO comb, spatial resolution could be significantly improved while reducing drastically the detection bandwidth requirements.

The limits in the performance of TE-φOTDR fundamentally depend on the characteristics of the generated OFCs. Achieving kilometer distances with centimeter resolutions, that is, having more than 10^4 sensing points, implies the creation of identical number of comb lines separated by less than 100 kHz. When considering a conventional dual-comb scheme, the need of accommodating such high quantity of lines within a very narrow RF bandwidth drastically restricts the measurement speed. This major drawback has been addressed by using two OFCs with a quasi-inter-ratio (QIR) relation between their repetition rates [33]. The subsequent dissimilarity in the periods of the combs makes it possible to speed up the refresh rate of the sensor by an integer factor, without drastically increasing the detection bandwidth. Thus, dynamic strain sensing over 2 km with 2 cm of spatial resolution (i.e., 100,000 sensing points) has been reported using TE-φOTDR in a QIR mode, still preserving a digitization rate of 100 MSa/s [34]. The total number of sensing points, however, ultimately depends on the

phase noise of the RF oscillator involved in the EO modulation. Therefore, increasing the sensor range (while preserving the spatial resolution) progressively imposes more stringent requirements in the frequency stability of the dual-comb generator [34].

In this paper, we overview the operation principle of TE-φOTDR in a phase-demodulation sensing approach, paying special attention to the existing trade-offs and performance limits of both the basic and the QIR configuration. We show representative results for strain and temperature sensing. Alternative schemes to simplify the TE-φOTDR implementation are briefly discussed, as well as further potential applications.

II. Operation Principles of TE-ΦOTDR

A. *Fiber interrogation using dual frequency combs*

As previously mentioned, TE-φOTDR combines the traditional DAS configuration based on phase-demodulation φOTDR with concepts borrowed from dual comb spectroscopy [29]. In particular, the interrogating probe signal is similar to that used in traditional φOTDR, e.g., a periodic train of pulses. This signal corresponds to an OFC in frequency domain. The optical bandwidth B_{opt} of the comb is inversely proportional to the pulse width and the comb line spacing is equal to the inverse of the pulse train period, $f_R = 1/T$, see Fig. 1(a) and (b). The number of comb lines $N = B_{opt} / f_R + 1 \approx B_{opt} / f_R$ matches the maximum number of individual sensor points delivered by the distributed sensor: $N = T/\tau = L_{\max}/\Delta z$. In this expression, τ is the pulse width, $L_{\max}$ is the maximum length of the interrogated fiber and Δz is the spatial resolution. The maximum length is limited by the pulse train period, $L_{\max} = T \cdot c/(2 \cdot n)$, where c is the speed of light in a vacuum and n the effective refractive index of the fiber. The spatial resolution, on its turn, is given by $\Delta z = c/(2 \cdot n \cdot B_{opt})$. The main difference with a traditional phase-demodulation φOTDR lies in the employed LO. In TE-φOTDR, the LO is not a continuous wave signal (i.e., a pure frequency tone), but another OFC with the same number of lines N than the probe comb and a slightly different line spacing, $f_R^{LO} = f_R + \delta f$, with $\delta f << f_R$ (Fig. 1(a)). Upon detection, the beating of both combs can be seen as a multi-heterodyne process, producing a series of beat notes distributed along the RF domain. The RF lines are clustered around multiplies of f_R. To guarantee unambiguous detection of the comb lines, it is important that the beating of probe-LO lines falls within spectral regions of width $f_R/2$ known as Nyquist zones. Avoiding the mixing of beat tones from different zones is ensured when the following condition is accomplished:

$$\delta f < \frac{f_R^2}{2B_{opt}}. \quad (1)$$

In this case, the complete information of the probe signal is bounded within the first Nyquist zone, so the detection bandwidth is limited to a narrow spectral region ($< f_R/2$). This frequency downconversion between the optical and electrical domains, is parametrized by the compression factor (CF), defined as $f_R/\delta f$ (Fig. 1(c)).

Assuming transform-limited combs, i.e., combs with constant or linear spectral phase profile, the time-domain probe and LO signals are trains of transform-limited (short) pulses. The envelope of such pulses is the inverse Fourier transform of the spectral comb envelope. The only difference between the signal and the LO is that the corresponding combs have a slightly different period ($1/f_R$ and $1/(f_R+\delta f)$, respectively, see Fig. 1(b)). The LO comb can be seen as a pulse train that performs a time gating. In this way, the interference of the probe pulse with the LO signal is equivalent to an asynchronous optical sampling (ASOPS) process [35]. The result is a discretized version of the probe pulse signal but expanded in time by a factor given by CF (Fig. 1(d)).

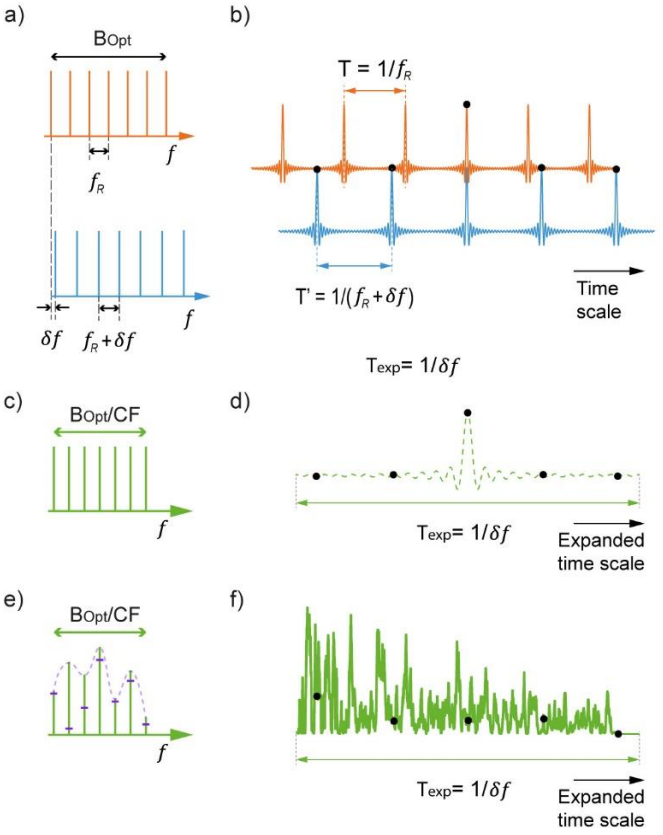

Fig. 1 (a) Frequency and (b) time-domain representations of a typical transform-limited optical DFC. Spectral (c) and time-domain representation (d) of the interference of both combs, corresponding to the spectral compression and time-expansion of the resulting waveform. Spectral (e) and time-domain representation (f) of the time-expanded trace produced by the interference of the backscattered signal and the LO. To facilitate the visualization of curves in (d) and (f), the drawing has been simplified by showing a limited number of sampling points.

Now let us assume that the probe signal is launched into the fiber under test (FUT). A train of backscattering traces is produced, which later interferes with the LO signal. Upon detection, a down-converted frequency comb encoding the amplitude and phase spectral response of the fiber is retrieved

from the first Nyquist zone (see purple dashed lines in Fig. 1(e)). In time-domain, the train of traces is optically sampled by the LO (Fig.1 (f)), generating a time-expanded trace whose duration is $1/\delta f$, which imposes an ultimate limit to the sampling rate of the sensing system. From Eq. (1), this duration, written in terms of N and T, is higher than $2NT$, evidencing the time expansion endowed by the proposed approach.

B. *Increasing the SNR through spectral coding*

Increasing the number of sensing points attained in TE-φOTDR requires pulses with a longer period (lower f_R) and/or shorter pulses (broader B_{opt}). This is equivalent to decrease the probe duty cycle. The peak power of the pulses cannot be arbitrarily high, since it is limited by the onset of nonlinear effects. Thus, improving the spatial resolution has a direct impact on the SNR of the retrieved traces, which scales with the average power sent to the fiber. The peak-to-average power ratio (PAPR) of transform-limited pulses (corresponding to an OFC with flat spectral phase) can be estimated as the inverse of the duty cycle, i.e., $PAPR \approx B_{opt}/f_R$. The value for the PAPR can be very high for low duty cycle pulse trains. For instance, when $B_{opt} = 5$ GHz and $f_R = 100$ kHz (the parameters of a sensor with a spatial resolution of 2 cm and a range of 1 km), PAPR=47 dB, which drastically limits the level of average power that can be injected into the fiber. Therefore, to improve the SNR while maintaining fine spatial resolution, it is necessary to include some kind of coding in the probe signal to decrease the PAPR.

In general, if the employed LO has identical coding than the probe signal, the beating between probe and LO induces an automatic decoding of the probe pulses [29], evading the need for post-processing decoding strategies (e.g., matched filtering [14-16]) and leading to a further simplification of the detection scheme. To date, several coding strategies have been applied in TE-φOTDR. In what follows, we describe the typical setup to generate arbitrary coded DFC for TE-φOTDR and we review the strategies so far employed.

1) *Employed setup for coded DFC in TE-φOTDR*

As introduced in the first section, we employ EO comb generation for TE-φOTDR, since it is an efficient approach to generate highly densified OFCs (with line spacing in the order of 100 kHz). EO combs also offer high flexibility to select their parameters depending on the requirements imposed by the sensing application. Another advantage of this OFC platform is the use of an arbitrary waveform generator (AWG) that enables an individual control of the amplitude and phase of the spectral lines of the combs. This capability has been harnessed to avoid the propagation of high-peak power probe pulses and, hence, to optimize the SNR of the detected signals, providing at the same time a straightforward sensing demodulation scheme [29]. The general TE-φOTDR setup configuration with EO-DFC generation is depicted in Fig. 2.

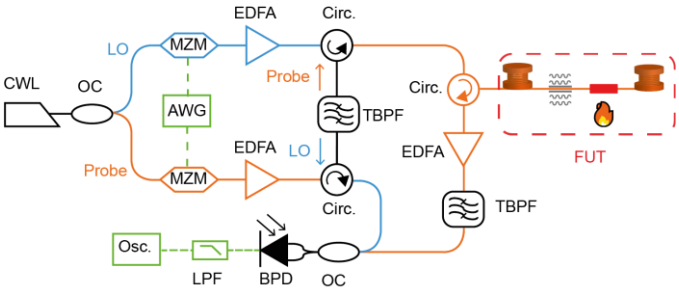

Fig. 2. Typical experimental setup employed for TE-φOTDR measurements. OC: optical coupler. The rest of the acronyms are defined through the text.

The optical combs are created thanks to a couple of Mach-Zehnder modulators (MZMs) that are optically fed by a low-phase-noise continuous wave laser (CWL). Electrically, the MZMs are driven by an AWG that produces a real-valued tailor-made signal, designed offline to generate OFCs with particular features. The spectrum of the modulating signal is composed of two symmetrical complex-conjugated sidebands around the optical carrier. At the output of the MZM, the dual-sided optical combs are amplified by two independent erbium-doped fiber amplifiers (EDFA) and filtered by a tunable band pass filter (TBPF). This filter not only reduces the amplified spontaneous emission (ASE) introduced by the EDFA but also suppresses one of the optical sidebands to ensure an unambiguous down conversion in detection. The TBPF is placed between two circulators so that the same device filters both the probe and LO combs. Hence, we ensure identical sideband and carrier suppression, as well as equal filter-induced phase in both combs, which will be cancel out in detection.

After filtering the combs, one of them (the probe comb) is launched into the fiber under test (FUT). The produced Rayleigh backscattering signal is collected by a circulator (Circ.) and then is amplified by another EDFA and filtered by a second TBPF. This filter only reduces the ASE introduced by the EDFA. The interference between the LO and probe combs is detected by a balanced photodetector (BPD). The resulting electrical signal is digitized and acquired by an oscilloscope (Osc.). An electrical low-pass filter (LPF) is usually placed after the BPD to reduce the sampling requirements for the Osc.

2) *Random spectral phase coding*

The first approach to codify the OFCs used in TE-φOTDR relies on the allocation of a random spectral phase profile in the comb lines [29]. In particular, the phase values are set to follow a uniform distribution between $-\pi$ and π. The introduction of this spectral phase coding changes the interference condition along the period of the signal, leading to the formation of a periodic speckle-like waveform in the time domain. As previously mentioned, the same spectral phase distribution is applied to the probe and LO combs, and hence, the compressed spectrum at the first Nyquist zone is automatically decoded, directly providing the impulse response of the probed fiber. The allocation of the random spectral phase has proved to reduce the PAPR from 27 dB (if transform-limited pulses are considered) down to 9 dB when using a comb with spectral characteristics suitable to attain thousands of sensing points in mid-length fiber ranges (i.e., 100s of meters) [29].

The first experimental demonstration employed two DFC composed of 5,000 lines (or equivalently, 5,000 measuring points) with a repetition rate f_R of 500 kHz. The resulting sensor was able to interrogate fibers up to around 200 m with a nominal spatial resolution of 4 cm (corresponding to 2.5 GHz of optical bandwidth). The offset between the repetition rate δf was set to 20 Hz and 40 Hz in two series of measurements. The effect of the phase coding was evaluated by calculating the SNR of a set of traces measured after probing a FUT of 154 m, as is shown in Fig. 3. In our experiments, the SNR was defined at each point of a trace as the ratio of the averaged power and its variance calculated over a certain time interval (e.g., 1s). The resulting values of the SNR were then averaged to obtain a representative estimation of the SNR for each trace. Thanks to the introduction of the random spectral phase in the employed combs, time-expanded traces for the FUT of 154 m were acquired with SNR of about 20 dB. With no phase coding, the SNR was insufficient to perform any sensing measurement (SNR< 3 dB). In this experimental demonstration, the effect of selecting different values for δf in the SNR of the traces was also checked. In particular, it was shown that reducing the offset δf increased the SNR in 3 dB. The price to pay is a reduction of sensing sampling rate by a factor of 2. Hence, modifying the offset between probe and LO acts exactly as an averaging process in terms of SNR and sensing bandwidth [29].

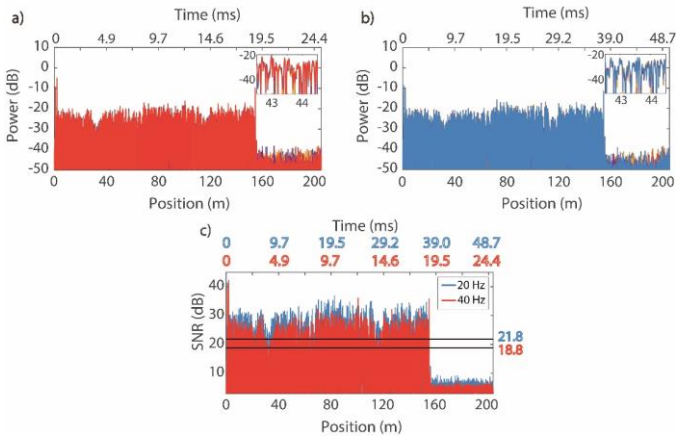

Fig. 3. Representative backscattering traces obtained with a comb composed of N = 5000 lines separated by f_R = 500 kHz with (a) an offset δf = 40 Hz and (b) δf = 20 Hz. The insets show a good repeatability of the recovered traces. The estimated SNR at each measured point is shown in (c) for δf = 40 Hz (red) and δf = 20 Hz (blue). Black lines in (c) refer to the average SNR value for each dataset. Figure extracted from Ref. [29].

By using random spectral phase coding, the sensing capabilities of the technique were also experimentally validated [29]. In particular, a new DFC was designed providing a nominal spatial resolution of 2 cm (B_{opt} = 5 GHz), while maintaining the maximum sensing range shown in the previous experiment (about 205 m). This supposes doubling the individual sensing points up to 10,000. A temperature measurement was carried out through the application of a hot spot of 2 cm around the position z = 122 m of the employed FUT. This hot point was implemented using a fiber cable with a pair of metallic wires embedded. A controlled electric current passed through 2 cm of the wire, varying the temperature of the optical fiber through Joule effect. The current was driven by a sinusoidal wave of 5 s of period, thus producing a periodical heating-cooling process. The retrieved temperature profile from the optical fiber around the hotspot is shown in Fig. 4. A well-defined 2 cm periodical perturbation was recovered. The average value of the temperature amplitude was 0.96ºC. The triangular shape of the perturbation shown in Fig. 4 (b) comes from the convolution between the square window defined by the gauge length and the square-shaped hot spot boundaries. The amplitude spectral density along the perturbed region (Fig. 4 (c)) shows that the frequency of the recovered perturbation matches the frequency of the applied perturbation (0.2 Hz). The estimated noise floor is 0.02 $rad/\sqrt{Hz}$. The calculated accuracy is 0.09 rad, which means 390 $n\varepsilon$ or equivalently 55 mK.

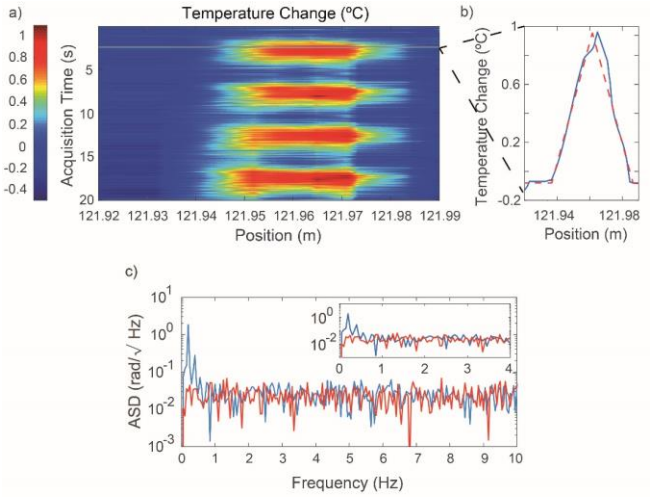

Fig. 4. a) Dynamic temperature map around a hot-spot. b) Detail of the thermal perturbation obtained experimentally (blue) and theoretically (dashed red line) c) Amplitude spectral density (ASD) in a representative position of the perturbation (blue line) and ASD in an unperturbed fiber region (red). Figure extracted from Ref. [29].

3) Optimized coding. Parabolic spectral phase profile

The random spectral phase coding employed in the first approach is far from being the most efficient coding strategy, since according to the random-walk formalism, the magnitude of the resulting temporal signal follows a Rayleigh distribution [29]. For this reason, a more elaborated coding strategy was proposed in [36]. This strategy consists of the allocation of a customized quadratic spectral phase on the comb lines. This phase is designed to accomplish the temporal far-field condition, resulting in a frequency-to-time mapping. If the comb spectrum has a flat topped (constant) envelope, the resulting time-domain signal is a square pulse whose duration can be set to fill the period of the signal ($1/f_R$). Mathematically, these combs are defined by:

$$E_{pr}(f) = E_0 \cdot \sum_{m=-N/2}^{N/2} \delta(f - m \cdot f_R) \cdot \exp\left\{ j \frac{\Psi(2\pi f)^2}{2} \right\} \qquad (2)$$

where m is an integer, f the frequency, E_0 the spectral amplitude of each comb line and Ψ the quadratic phase parameter. The duration of the pulses is given by $\Psi 2\pi B_{opt}$. To fill the entire period of the signal, the quadratic parameter is calculated as:

$$\Psi = \frac{1/f_R}{2\pi B_{Opt}} \quad (3)$$

Experimentally, the optimal value Ψ_{opt} for this parameter is a bit smaller than the one given by Eq. 3 (around $0.95\cdot\Psi$) due to the interference that takes place between the tails of different pulses. Compared to other spectral phase coding configurations (namely, flat and random spectral profiles) the quadratic phase reduces the PAPR to nearly 0dB, reaching a time-domain signal with almost continuous magnitude. Empirically, the PAPR is about 2 dB due to the mentioned interference between the tails of consecutive pulses.

We performed an experiment to verify the improvement in SNR provided by this highly-energy efficient coding approach. We used a setup similar to that presented in Fig. 2. In particular, four different DFC configurations were designed. All of them had N = 500 lines separated by f_R = 10 MHz, thus providing a measurable range of 10 m and a spatial resolution of 2 cm (B_{opt} = 5 GHz). The first couple of DFCs had an offset of 2 kHz. This value was increased up to 8 kHz for the other couple. One configuration of each couple was designed with a random spectral phase coding, while a customized quadratic phase profile was allocated in the other DFC. The interrogated FUT had 3.56 m where 2 cm were mechanically perturbed by a shaker. This shaker was driven by a sinusoidal signal of 500 Hz. The comb with random spectral phase resulted to have a PAPR of 9 dB, while this was reduced until 2 dB for the configurations with quadratic spectral phase. The strain map around the perturbed point in each case is shown in Fig. 5. Left (right) figures were obtained using quadratic (random) spectral phases, while the first (second) row corresponds to δf = 2 kHz (δf = 8 kHz).

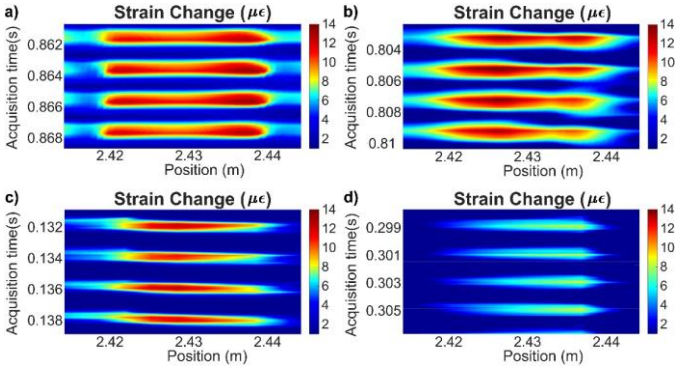

Fig. 5. Strain map evolution around the perturbation where a the employed DFC has δf = 2 kHz and quadratic spectral phase coding, (b) δf = 2 kHz and random spectral phase coding, (c) δf = 8 kHz and quadratic spectral phase coding and (d) δf = 8 kHz and random spectral phase coding. Figure published in [36].

We recovered a well-defined perturbation in Fig. 5 (a), (b) and (c). However, in Fig. 5 (d), the quality of the recovery was clearly worse. This loss of fidelity can be attributed to the degradation of the SNR when the acoustic sampling is increased (Section II.B.2). The performance upgrade related to the PAPR improvement was also observed in the noise floor values obtained from the power spectral density (PSD) calculated for the four mentioned perturbations, as can be observed in Table 1. This table also includes the PSD values corresponding to the perturbation frequency (500 Hz). Regardless the value of δf, the noise floor values obtained with the combs having the quadratic phase (QP) were 6 dB lower than those obtained with random phase (RP). Furthermore, with QP coding, the SNR was improved in 7 dB and 8 dB for δf = 2 kHz and δf = 8 kHz, respectively. These SNR improvements are in line with the PAPR reduction obtained when comparing both spectral phase coding approaches.

Table 1. List of values for the noise floor and signal peaks for different codifications and acoustic samplings. Table extracted from [36]

	2 kHz		8 kHz	
	QP	RP	QP	RP
Signal peak (dB rel. 1 rad²/Hz)	-3.9	-4.3	-0.93	-2.8
Noise Floor (dB rel. 1 rad²/Hz)	-54.8	-48.3	-54.8	-48.7
SNR (dB)	50.9	44	53.9	45.9

QP: quadratic phase, RP: random phase.

C. *Simplified, cost-efficient TE-φOTDR schemes*

In all configurations detailed in the previous Sections, the generated DFCs have been based on phase spectral modulation of constant amplitude lines, thus avoiding the formation of low duty cycle trains of pulses. However, the generation of such a specific time-domain RF signals has required the use of a high sampling rate AWG, which in turn increases the complexity and cost of the sensing system. Two alternative, lower-cost DFC generation schemes have been tested in TE-φOTDR.

The first scheme is based on the EO generation of comb through the use of pseudo-random bit sequences (PRBS) [37]. Nowadays, inexpensive and readily embeddable PRBS cards are available in the market, able to attain optical bandwidths of tens of GHz (i.e., providing sub-cm spatial resolutions in TE-φOTDR). The code length of the generated PRBS sequence fixes the number of lines of the combs, in turn limiting the attainable range once the bandwidth is fixed. Using a 2^{15}-1 length PRBS sequence at 11 Gbps, we demonstrated a TE-φOTDR configuration attaining spatial resolutions of around 1 cm with 15,000 independent measure points and about 150 m sensing fiber length. We performed a temperature measurement test, achieving an accuracy of 0.142ºC [37].

The above-mentioned approach still needs a high frequency oscillator that matches the targeted optical bandwidths of the combs (e.g., of several GHz). In a second approach, step recovery diodes (SRD) were employed to implement the dual-comb architecture [38]. This scheme requires an oscillator

whose frequency matches the required comb line spacing, enabling the implementation of a high-resolution sensing system employing only low-frequency electronics (e.g., in MHz regime). The main disadvantage of the use of SRDs is that the generated combs are nearly transform-limited, hampering the improvement of SNR due the lack of a spectral phase coding. Still, using this strategy, distributed strain sensing capability over a range of 20 m, spatial resolution of 3 cm and acoustic sampling rate of 200 Hz was demonstrated, requiring electronics with frequencies of just a few MHz.

III. Quasi-Integer-Ratio Configuration

A. *Relaxing performance trade-offs in TE-φOTDR*

Unambiguous spectral compression using DFCs imposes stringent trade-offs between the offset δf, the line spacing f_R and the bandwidth B_{opt} to avoid aliasing between beat frequencies in detection (see Eq. 1). Ideally, δf should be large (high sensing sampling rate), f_R should be low (long range), B_{opt} should be large (fine resolution), and the ratio B_{opt}/f_R should be large (number of sensing points). In principle, all these conditions cannot be achieved at the same time. To better illustrate this problem through numerical examples, if a high number of sensing points is pursued (e.g., 10,000 points), the sensing bandwidth is necessarily reduced (e.g., 25 Hz, considering 2 cm resolution, corresponding to B_{opt} = 5 GHz). On the other hand, fine resolution and high sampling frequency (e.g., 2 cm resolution and 1 kHz) is only reachable in short fibers (e.g., less than 32 m).

The above performance limitations can be significantly relaxed if another concept from dual comb spectroscopy is implemented, namely, DFC with quasi-integer-ratio repetitions rates, or in short, QIR-DFC [33]. In this alternative scheme, a probe frequency comb with the desired features in terms of bandwidth and line spacing is generated. However, unlike the conventional DFC configuration described in Section II.A, the LO comb is not a frequency comb similar to the probe, with the same number of lines and a line spacing only differing in a small offset. Instead, the LO is a comb whose line spacing is a quasi-integer multiple of the probe line spacing, that is, $f_R^{LO} = M \cdot f_R + \delta f$, with M being a positive integer known as the quasi-integer factor [29,33]. This selection for the LO comb has several implications: the number of the lines of the LO comb is reduced by a factor *M*, the Nyquist zones in the RF domain are composed of approximately M/N lines and the acquisition of N lines of the probe requires the detection of M Nyquist zones. The fact that the Nyquist zones have a smaller number of lines than in the original situation (in which M =1) relaxes the condition to avoid aliasing in detection to

$$\delta f < M \cdot \frac{f_R^2}{2B_{opt}}. \quad (4)$$

Again, to provide a numerical example of the possibilities of this technique in distributed sensing, we could target fine resolution of 2 cm (B_{opt} = 5 GHz) and sampling frequency of 1 kHz over a fiber of up to 547 m for M = 300. The price to pay for speeding up the measurement rate is an increase of detection bandwidth. Since M Nyquist zones are to be detected, the photodetection bandwidth must be now $B_{RF} = M \cdot f_R$ (<55 MHz in the example, still two orders of magnitude lower than the bandwidth imposed by the target resolution).

QIR-TE-φOTDR has proven sensing capabilities ranging between traditional phase-demodulation φOTDR and OFDR, which has typically lower sampling rate for long fibers. A detailed comparison between these techniques can be found in [29]. In this section, we review the time-domain interpretation and recent developments in QIR-TE-φOTDR technology.

B. *Frequency analysis of acquired signals in the QIR mode*

As explained in Sec. II.A, the probe comb samples the spectral frequency response of the fiber, producing backscattering traces. The resulting backscattered comb beats with the LO, producing a multiheterodyne process upon detection. However, in QIR-TE-φOTDR, instead of having a one-to-one relationship between probe and LO lines, the p th line of the LO acts as a reference for the $\left[(p-1)M+1, pM\right]$ lines of the probe comb (see Fig. 6). The sliced multiheterodyne process in QIR-TE-φOTDR induces a disordering of the spectral lines in the RF domain. In general, the offset of the n th line of the backscattered comb from the baseband is $\mathrm{mod}(M-n, M)\cdot f_R + p\cdot\delta f$, where mod is the remainder after division of $M-n$ and M. To recover the spatial information correctly, it is required to re-arrange the beat lines (Fig. 6(b) and (c)).

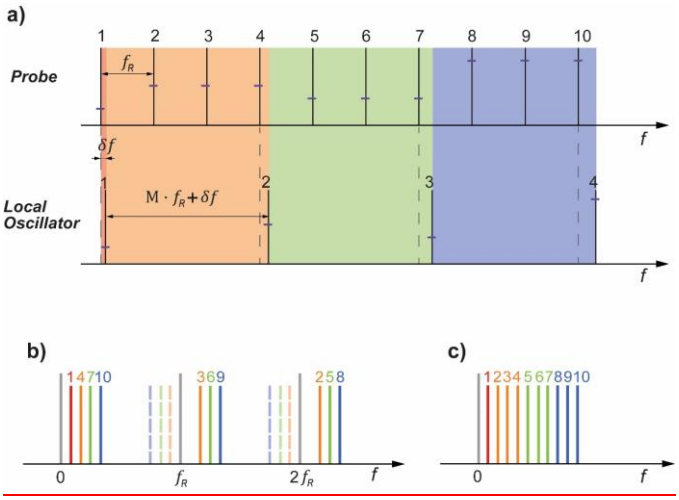

Fig. 6. Frequency domain representation of the QIR-DFC scheme. (a) The probe and the LO combs cover similar optical bandwidth but with a different number of teeth. (b) The interference of both combs generates groups of lines (Nyquist zones) on which the response of the probe is encoded. (c) After rearranging the lines, a down-converted version of the probe comb can be obtained. Figure extracted from Ref. [29].

In time domain, the multiheterodyne detection process described above is equivalent to a re-ordering of the samples in the time-domain interferograms when the ASOPS of the traces is performed with a LO. As is shown in Fig. 7, the faster (LO)

comb samples each period of the slower (probe) comb N/M times. Hence, the spatial information is fully acquired after sampling M periods of the probe comb, so the time-expansion factor is reduced in a factor of M. The samples acquired at each of the periods of the slower comb go to a different Nyquist zone. In this way, the time-domain signal resulting from the inverse Fourier transform of each Nyquist zone corresponds to a downsampled version of the complete period, having an offset in the sampling time of $M/(N\cdot\delta f)$ seconds. To reconstruct the original signal, the M downsampled traces have to be interleaved.

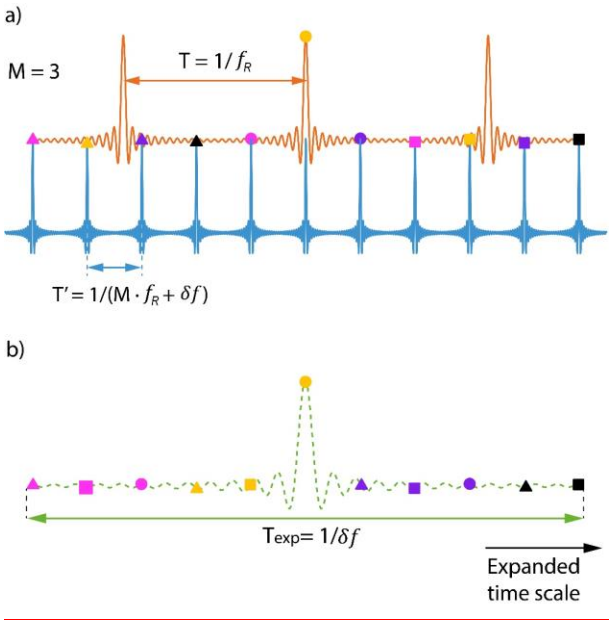

Fig. 7. (a) Time-domain interpretation of the QIR-DFC configuration. The faster LO comb samples each period of the comb probe N/M times. (b) The temporal samples of M periods of the probe comb need to be interleaved to reconstruct the complete period over an expanded time scale.

C. *Spectral phase coding in QIR-TE-φOTDR*

In the original version of TE-φOTDR, where M =1, the coding strategies always consider a one-to-one relationship in the spectral phases of the LO and probe combs. Therefore, upon detection, the phase spectral coding applied to the probe comb is automatically decoded by the LO. In order to obtain automatic decoding in QIR-TE-φOTDR, the spectral phase of the pth line of the LO must be equal than the phase of the $\left[(p-1)M+1, pM\right]$ lines of the probe comb (see Fig. 6 (a)).

The fact that a group of M lines of the probe comb has the same spectral phase increases the PAPR of the time domain probe signal, in turn decreasing the SNR of the backscattered traces. To date, all experimental demonstrations of QIR-TE-φOTDR have been done using this approach (automatic phase decoding). Post-processing techniques capable of inducing an arbitrary phase spectral coding to the probe comb lines are currently under investigation.

D. *Frequency stability requirements in QIR-TE-φOTDR*

The disordering of comb tones induced by the multi-heterodyne process has an important consequence in terms of the frequency stability requirements of QIR-TE-φOTDR. In the literature, it has been demonstrated that, when using EO comb generation techniques, the three main noise sources that degrade the signal fidelity are optical noise from laser and optical amplifiers, electrical noise and photodiode noise [39]. When considering a DFC configuration, and assuming the use of a laser with sufficiently narrow linewidth (i.e., whose coherence length is significantly longer than the difference in the optical path length between the two combs), the main source of noise is given by the relative frequency noise between the two combs. In Ref. [34], we demonstrated an upper bound for the frequency stability of the clock employed as a reference in the comb generation process. This limit was obtained under three assumptions. First, the two combs of the DFC are generated from a common oscillator (e.g., through a phase locked loop).

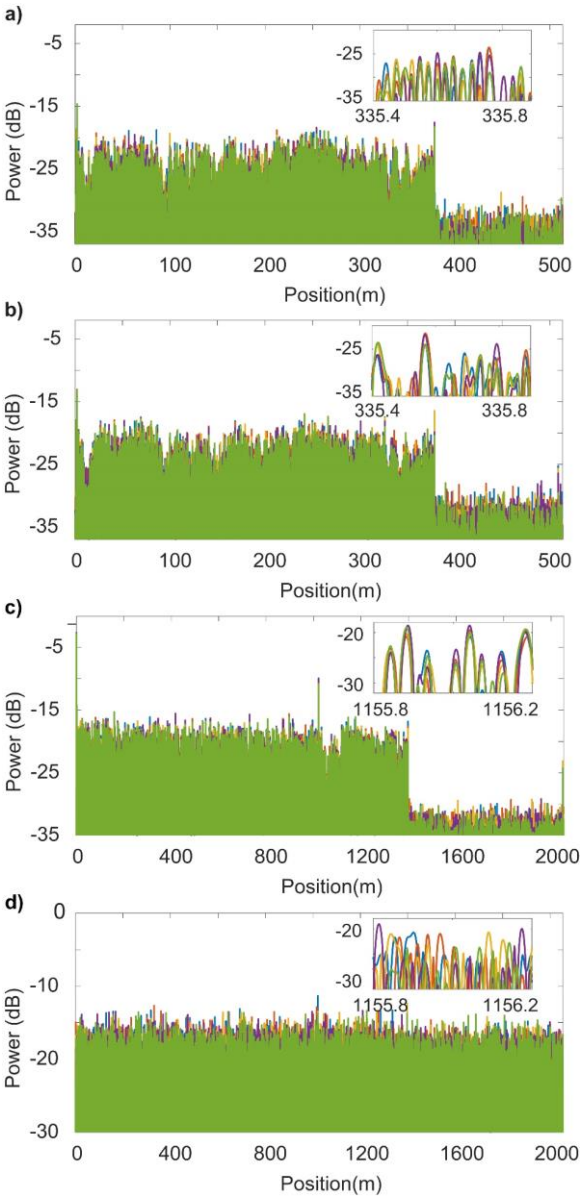

Fig. 8. Time-expanded traces recovered after spectral re-ordering employing a QIR-DFC with f_R = 200 kHz and M = 320 (a, b) and f_R = 50 kHz and M = 400 (c,d). A rubidium clock is employed in (a) and (c), while an OCXO is

applied in (b) and (d). Insets show a zoom of an unperturbed region around the end of the traces to show repeatability. Figure extracted from Ref. [34].

Second, the comb parameters M and N are both much higher than 1 and the Nyquist zone are supposed to be almost completely filled ($\delta f \approx M \cdot f_R^2 / (2B_{opt})$). Third, the maximum frequency error affordable in a measurement is that making the integrated jitter much lower than the duration of one measurement point, i.e., $\Delta T_{max} \approx 1/(N \cdot \delta f)$. Hence, the upper bound for the relative frequency error of the reference oscillator (i.e., for the frequency stability of the clock) in QIR-TE-φOTDR is given by

$$\varsigma_{clock} \approx \frac{1}{2 \cdot N^2}. \quad (5)$$

This condition contrasts with the required clock frequency stability in the original TE-φOTDR system (M =1), where $\varsigma_{clock} \approx 1/N$ [34]. Hence, in the QIR case, the stability condition is a factor of $2N$ more stringent. This corresponds with the fact that, upon reordering, some low-frequency components have $2N$ times larger frequency noise than in the conventional TE-φOTDR scheme, since their original beating frequency was about $2N$ times larger than the sampling frequency (δf) (nearly at the upper edge of the RF spectrum).

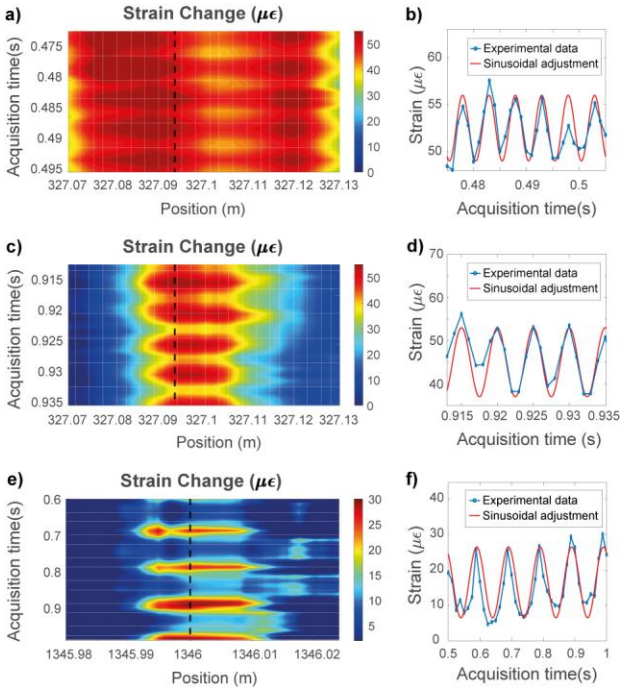

Fig. 9. Strain map around the perturbed section for the dual-comb configuration with N = 25,000 employing the OCXO reference clock (a) and temporal evolution of the strain at the position marked with dashed line (b). Same measurement using the rubidium clock in (c) and (d), respectively. Strain map around the perturbation for the dual-comb with N = 100,000 lines employing the rubidium clock as reference (e). Temporal evolution of the strain in the marked point (f). Figure extracted from Ref. [34].

To experimentally validate the attained result, two different reference clocks were employed in a QIR-TE-φOTDR configuration. One clock was an oven-controlled crystal oscillator (OCXO) with relative stability in the order of 10^{-9}. The second clock was a rubidium oscillator linked to a GPS signal (TimeTech GPS 5.10) that presented a relative frequency stability of 10^{-13} in short times. According to Eq. 5, those clocks would be useful for implementing a QIR-TE-φOTDR system of 22,000 and 2,200,000 lines, respectively. Two different configurations were tested, one targeting 25,000 sensing points and one targeting 100,000 sensing points. The first configuration was aimed at interrogating 500 m of fiber with 2 cm resolution and 1 kHz of perturbation sampling rate. The QIR factor was M =320. The FUT had a length of 378 m. The periodic perturbation was applied over 2 cm and had a frequency of 200 Hz. The second configuration was aimed at interrogating a fiber of 2 km with a sampling rate of 80 Hz. The probe comb had again 5 GHz bandwidth with a line spacing of 50 kHz. The QIR factor was M = 400. The length of the FUT was 1390 m and the applied perturbation had a frequency of 10 Hz.

The obtained results proved that, even if the SNR of the traces was relatively high, the effect of the lack of sufficient frequency stability induces a jitter on the traces that vanishes their mutual coherence, challenging the reconstruction of a perturbation from them (see insets of Fig. 8). Only in those cases where the condition shown in Eq. 5 was satisfied by using the rubidium clock (Fig. 8(a) and (c)), a strain perturbation could be properly resolved in space (Fig. 9(c) and (e)) [34]. With the OCXO, the first comb configuration could detect a periodic perturbation but poorly resolved in space (Fig. 9(a)). This effect is attributed to the integrated jitter along the trace, which "spreads" the perturbed region. The estimated noise floor in a sensing measurement using the first configuration (N = 25,000) was -18.8 and -21.7 dB ref. 1 $\mu\varepsilon^2$/Hz [40] when using the OCXO and the rubidium clock, respectively. For the second configuration (N = 100,000), the noise floor was -11.5 dB ref. 1 $\mu\varepsilon^2$/Hz when using the rubidium clock, while it was impossible to recover a meaningful measurement with the OCXO.

IV. Conclusions

In this work, we have revisited a novel DOFS technique based on dual comb interferometry, namely TE-φOTDR. The fundamental principle of this technique is similar to that of phase-demodulated φOTDR with coded pulses. The main difference with this previous technique lies in the employed LO. While in conventional φOTDR the LO is a continuous wave signal, in TE-φOTDR, the LO is a signal identical to the probe except for a slight difference in its period. This detuning induces an asynchronous sampling process with two main effects: (i) the duration of the detected optical traces is expanded in a configurable fashion, and (ii) the LO itself acts as a matched filter that automatically decodes the trace, directly providing the impulse response of the fiber with essentially optimal SNR. In consequence, TE-φOTDR arises as a powerful distributed sensing technique able to provide real time monitoring of strain and temperature with very high resolution (at cm level), relatively high range (100 m) and sampling rates of around 100 Hz, and all this with an astonishing reduced detection and acquisition bandwidth, potentially lower than 1 MHz. The performance of the technique can be further increased if the QIR configuration is employed. By using this configuration, we can readily reach kilohertz sampling rates

while keeping the mentioned resolution and range, or, alternatively, attain kilometer ranges if maintaining the resolution and sampling frequency. The detection bandwidth requirements in the QIR case are increased in one or two orders of magnitude (depending on the employed quasi-integer factor) but is still several orders of magnitude lower than in a traditional φOTDR targeting a centimeter resolution. Although so far, we have only used this technique for performing dynamic phase measurements (with its inherent limitations in terms of temperature/strain range), it is in principle immediate to extend it to wavelength-scanned φOTDR. This could provide larger ranges for the strain/temperature measurement at the expense of decreasing the measurement speed.

In conclusion, we foresee that this technique may become an important new tool in expanding all the benefits and advantages of distributed acoustic sensing to new scopes of operation in short-to-middle range applications. TE-φOTDR offers a dense sensor cluster with highly customizable performances while guaranteeing the usual advantages of optical fibers like mechanical flexibility, low size, lightweight, simplicity to be embedded in different materials, etc.

REFERENCES

[1]. A. Masoudi and T. P. Newson, "Contributed Review: Distributed optical fibre dynamic strain sensing," *Rev. Sci. Instrum.*, vol. 87, no. 1, pp. 011501, Jan. 2016.

[2]. P. Lu, N. Lalam, M. Badar, B. Liu, B. T. Chorpening, M. P. Buric, and P. R. Ohodnicki, "Distributed optical fiber sensing: Review and perspective," *Appl. Phys. Rev*., vol. 6, no. 4, pp. 041302, Oct. 2019.

[3]. Z. He and Q. Liu, "Optical Fiber Distributed Acoustic Sensors: A Review," *J. Light. Technol*., vol. 39, no. 12, pp. 3671–3686, Jun. 2021.

[4]. D. Chen, Q. Liu, and Z. He, "108-km Distributed Acoustic Sensor with 220-pε/Hz Strain Resolution and 5-m Spatial Resolution," *J. Light. Technol*., vol. 37, no. 18, pp. 4462–4468, Feb. 2019.

[5]. J. C. Juarez, E. W. Maier, K. N. Choi, and H. F. Taylor, "Distributed fiber-optic intrusion sensor system," *J. Light. Technol*., vol. 23, no. 6, pp. 2081–2087, Jun. 2005.

[6]. P. G. Hubbard, J. Xu, S. Zhang, M. Dejong, L. Luo, K. Soga, C. Papa, C. Zulberti, D. Malara, F. Fugazzotto, F. Garcia Lopez, and C. Minto, "Dynamic structural health monitoring of a model wind turbine tower using distributed acoustic sensing (DAS)," *J. Civ. Struct. Heal. Monit*., vol. 11, pp. 833–849, May 2021.

[7]. J. Zuo, Y. Zhang, H. Xu, X. Zhu, Z. Zhao, X. Wei, and X. Wang, "Pipeline Leak Detection Technology Based on Distributed Optical Fiber Acoustic Sensing System," *IEEE Access*, vol. 8, pp. 30789–30796, Feb. 2020.

[8]. Z. Zhan, "Distributed acoustic sensing turns fiber-optic cables into sensitive seismic antennas," *Seismol. Res. Lett*., vol. 91, no. 1, pp. 1–15, Jan. 2020.

[9]. Y. Lu, T. Zhu, L. Chen, and X. Bao, "Distributed vibration sensor based on coherent detection of phase-OTDR," *J. Light. Techno*l., vol. 28, no. 22, pp. 3243–3249, Nov. 2010.

[10]. A. Masoudi, M. Belal, and T. P. Newson, "A distributed optical fibre dynamic strain sensor based on phase-OTDR," *Meas. Sci. Technol*., vol. 24, no. 8, pp. 085204, Jul. 2013.

[11]. J. Pastor-Graells, H. F. Martins, A. Garcia-Ruiz, S. Martin-Lopez, and M. Gonzalez-Herraez, "Single-shot distributed temperature and strain tracking using direct detection phase-sensitive OTDR with chirped pulses," *Opt. Express*, vol. 24, no. 12, pp. 13121–13133, Jun. 2016.

[12]. X. He, S. Xie, F. Liu, S. Cao, L. Gu, X. Zheng, and M. Zhang, "Multi-event waveform-retrieved distributed optical fiber acoustic sensor using dual-pulse heterodyne phase-sensitive OTDR," *Opt. Lett*., vol. 42, no. 3, pp. 442–445, Jan. 2017.

[13]. H. F. Martins, S. Martin-Lopez, P. Corredera, P.Salgado, O. Frazão, and M. González-Herráez, "Modulation instability-induced fading in phase-sensitive optical time-domain reflectometry," *Opt. Lett*., vol. 38, no. 6, pp. 872-874, Mar. 2013.

[14]. H. F. Martins, K. Shi, B. C. Thomsen, S. Martin-Lopez, M. Gonzalez-Herraez, and S. J. Savory, "Real time dynamic strain monitoring of optical links using the backreflection of live PSK data," *Opt. Express*, vol. 24, no. 19, pp. 322–328, Sep. 2016.

[15]. W. Zou, S. Yang, X. Long, and J. Chen, "Optical pulse compression reflectometry: proposal and proof-of-concept experiment," *Opt. Express*, vol. 23, no. 1, pp. 512-522, Jan. 2015.

[16]. Z. Wang, B. Zhang, J. Xiong, Y. Fu, S. Lin, J. Jiang, Y. Chen, Y. Wu, Q. Meng, and Y. Rao, "Distributed acoustic sensing based on pulse-coding phase-sensitive OTDR," *IEEE Internet Things J*., vol. 6, no. 4, pp. 6117–6124, Aug. 2018.

[17]. D. Arbel and A. Eyal, "Dynamic optical frequency domain reflectometry," *Opt. Express*, vol. 22, no. 8, pp. 8823-8830, Apr. 2014.

[18]. L. Marcon, A. Galtarossa, and L. Palmieri, "High-frequency high-resolution distributed acoustic sensing by optical frequency domain reflectometry," *Opt. Express*, vol. 27, no. 10, pp. 13923-13933, May 2019.

[19]. S. A. Diddams, K. Vahala, and T. Udem, "Optical frequency combs: Coherently uniting the electromagnetic spectrum," *Science*, vol. 369, no. 6501, pp. 1-12, Jul. 2020.

[20]. I. Coddington, W. C. Swann, and N. R. Newbury, "Coherent multiheterodyne spectroscopy using stabilized optical frequency combs," *Phys. Rev. Lett.*, vol. 100, no. 1, pp. 013902, Jan. 2008.

[21]. I. Coddington, W. Swann, and N. Newbury, "Coherent dual-comb spectroscopy at high signal-to-noise ratio," *Phys. Rev. A*, vol. 82, no. 4, pp. 043817, Oct. 2010.

[22]. D. A. Long, A. J. Fleisher, K. O. Douglass, S. E. Maxwell, K. Bielska, J. T. Hodges, and D. F. Plusquellic, "Multiheterodyne spectroscopy with optical frequency combs generated from a continuous-wave laser," *Opt. Lett*., vol. 39, no. 9, pp. 2688–2690, May 2014.

[23]. V. Duran, L. Djevarhidjian, and H. Guillet de Chatellus, "Bidirectional frequency-shifting loop for dual-comb spectroscopy," *Opt. Lett.*, vol. 44, no. 15, pp. 3789–3792, Jul. 2019.

[24]. C. Quevedo-Galán, V. Durán, A. Rosado, A. Pérez-Serrano, J. M. G. Tijero, and I. Esquivias, "Gain-switched semiconductor lasers with pulsed excitation and optical injection for dual-comb spectroscopy," *Opt. Express*, vol. 28, no. 22, pp. 33307–33317, Oct. 2020.

[25]. Y. Bao, X. Yi, Z. Li, Q. Chen, J. Li, X. Fan, and X. Zhang, "A digitally generated ultrafine optical frequency comb for spectral measurements with 0.01-pm resolution and 0.7-μs response time," *Light Sci. Appl*., vol. 4, no. e300, pp. 1-7, Mar. 2015.

[26]. G. Millot, S. Pitois, M. Yan, T. Hovannysyan, A. Bendahmane, T. W. Hänsch, and N. Picqué, "Frequency-agile dual-comb spectroscopy," *Nat. Photonics*, vol. 10, pp. 27–30, Dec. 2016.

[27]. K. Fdil, V. Michaud-Belleau, N. B. Hébert, P. Guay, A. J. Fleisher, J.-D. Deschênes, and J. Genest, "Dual electro-optic frequency comb spectroscopy using pseudo-random modulation," *Opt. Lett*., vol. 44, no. 17, pp. 4415–4418, Aug. 2019.

[28]. M. Soriano-Amat, M. A. Soto, V. Duran, H. F. Martins, S. Martin-lopez, M. Gonzalez-herraez, and M. R. Fernández-ruiz, "Common-Path Dual-Comb Spectroscopy Using a Single Electro-Optic Modulator," *J. Light. Technol.*, vol. 38, no. 18, pp. 5107–5115, May 2020.

[29]. M. Soriano-Amat, H. F. Martins, V. Durán, L. Costa, S. Martin-Lopez, M. Gonzalez-Herraez, and M. R. Fernández-Ruiz, "Time-expanded phase-sensitive optical time-domain reflectometry," *Light Sci. Appl*., vol. 10, no. 51, pp. 1-12, Mar. 2021.

[30]. M. Gonzalez-Herraez, M. Soriano-Amat, V. Durán, H. F. Martins, S. Martin-Lopez, and M. R. Fernández-Ruiz, "Time-Expansion in Distributed Optical Fibre Sensing," in *26th Optoelectronics and Communications Conference* (2021), paper W4D.4.

[31]. Y. Koyamada, M. Imahama, K. Kubota and K. Hogari, "Fiber-optic distributed strain and temperature sensing with very high measurand resolution over long range using coherent OTDR," J. Ligthw. Technol., vol. 27, no. 9, pp. 1142-1146, May 2009.

[32]. X. Lu, M. A. Soto, L. Zhang and L. Thévenaz, "Spectral properties of the signal in phase-sensitive optical time-domain reflectometry with direct detection," *J. Ligthw. Technol*., vol. 38, no. 6, pp. 1513-1521, Feb. 2020.

[33]. N. B. Hébert, S. Boudreau, J. Genest, and J.-D. Deschênes, "Coherent dual-comb interferometry with quasi-integer-ratio repetition rates," *Opt. Express*, vol. 22, no. 23, pp. 29152–29160, Nov. 2014.

[34]. M. Soriano-Amat, H. F. Martins, V. Durán, P. Fermoso, S. Martin-Lopez, M. Gonzalez-Herraez, and M. R. Fernández-Ruiz, "Frequency stability requirements in quasi-integer-ratio time-expanded phase-sensitive OTDR," *J. Ligthw. Technol.*, vol. 41, no. 2, pp. 777-783, Jan. 2023.

[35]. A. Bartels, R. Cerna, C. Kistner, A. Thoma, F. Hudert, C. Janke, and T. Dekorsy, "Ultrafast time-domain spectroscopy based on high-speed asynchronous optical sampling," *Rev. Sci. Instrum.*, vol. 78, no. 3, pp. 035107, Mar. 2007.

[36]. M. Soriano-Amat, H. F. Martins, V. Durán, S. Martin-Lopez, M. Gonzalez-Herraez, and M. R. Fernández-Ruiz, "Quadratic phase coding for SNR improvement in time-expanded phase-sensitive OTDR," *Opt. Lett*., vol. 46, no. 17, pp. 4406–4409, Sep. 2021.

[37]. J. Preciado, M. Soriano-Amat, P. Sevillano, D. Izquierdo, H. F. Martins, S. Martin-Lopez, M. Gonzalez-Herraez, M. R. Fernández-Ruiz and J.J. Martínez, "Time-expanded Φ-OTDR based on binary sequences," *IEEE Photon. Technol. Lett.*, vol. 34, no. 13, pp. 695-698, Jul. 2022.

[38]. M. Soriano-Amat, H. F. Martins, S. Martin-Lopez, M. Gonzalez-Herraez, M. R. Fernández-Ruiz, and V. Durán, "Time-expanded φOTDR using low-frequency electronics," *Opt. Express*, vol. 31, no. 2, pp. 843- 852, Jan. 2023.

[39]. C. Deakin, Z. Zhou, and Z. Liu, "Phase noise of electro-optic dual frequency combs," *Opt. Lett*., vol. 46, no. 6, pp. 1345–1348, Mar. 2021.

[40]. The units correspond to decibels referred to 1 $\mu\varepsilon^2$/Hz. That is: $10 \cdot log_{10}(PSD\ of\ strain/(1\ \mu\varepsilon)^2)$